



Lawrence Berkeley Laboratory

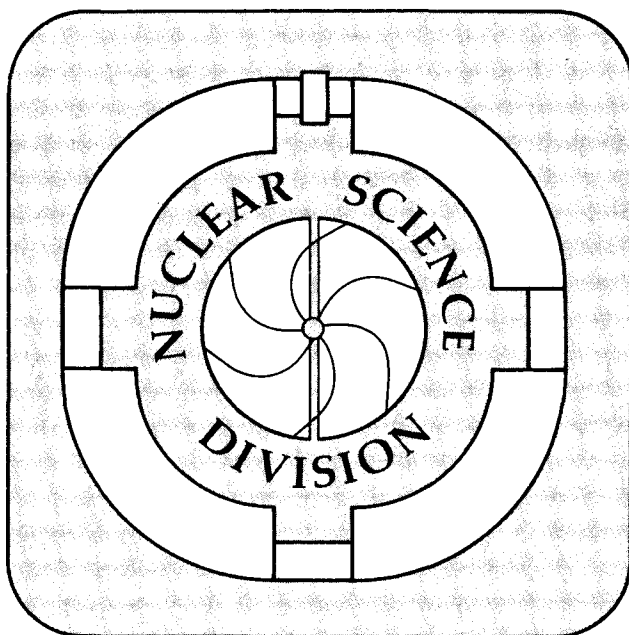
UNIVERSITY OF CALIFORNIA

Submitted to Physical Review C

Thermostatic Properties of Seyler-Blanchard Nuclei

E. de Lima Medeiros and J. Randrup

May 1991



LBL-30802
LOAN COPY
Circulates
for 4 weeks
Bldg. 50 Library.
Copy 2

DISCLAIMER

This document was prepared as an account of work sponsored by the United States Government. While this document is believed to contain correct information, neither the United States Government nor any agency thereof, nor the Regents of the University of California, nor any of their employees, makes any warranty, express or implied, or assumes any legal responsibility for the accuracy, completeness, or usefulness of any information, apparatus, product, or process disclosed, or represents that its use would not infringe privately owned rights. Reference herein to any specific commercial product, process, or service by its trade name, trademark, manufacturer, or otherwise, does not necessarily constitute or imply its endorsement, recommendation, or favoring by the United States Government or any agency thereof, or the Regents of the University of California. The views and opinions of authors expressed herein do not necessarily state or reflect those of the United States Government or any agency thereof or the Regents of the University of California.

Thermostatic Properties of Seyler-Blanchard Nuclei *

Emil de Lima Medeiros[†]

Centro Brasileiro de Pesquisas Físicas - CBPF
Conselho Nacional de Desenvolvimento Científico e Tecnológico - CNPq
22.290 Rio de Janeiro, RJ - Brazil

Jørgen Randrup

Nuclear Science Division, Lawrence Berkeley Laboratory
University of California, Berkeley, California 94720

May 29, 1991

ABSTRACT:

Employing a recently developed semi-classical nuclear model, based on a modified Seyler-Blanchard interaction depending on both momentum and density, we consider the thermostatic properties of hot isosymmetric nuclei embedded in a nucleon vapor. The level-density parameter is calculated and discussed. Simple analytical expansions are obtained for the dependence of the level-density parameter and the free energy on nuclear mass number and the temperature of the surrounding vapor. The model is employed for an illustrative study of the symmetric breakup of ^{120}Sn into a number of equal fragments.

*This work was supported in part by the Director, Office of Energy Research, Office of High Energy and Nuclear Physics, Nuclear Physics Division of the U.S. Department of Energy under Contract No. DE-AC03-76SF00098.

[†]Fellow, Brazilian Conselho Nacional de Desenvolvimento Científico e Tecnológico - CNPq, Contract No. 20.2057/89.5.

1 Introduction

Nuclear collisions at intermediate energies generate complex transient environments whose study may provide insight into both static and dynamical properties of systems under extraordinary conditions. In recent years considerable work has been devoted to this topic, and there has been significant progress with respect to producing and observing such processes. The experimental advances, in turn, have made increasing demands on theory and developments are presently underway over a broad front.

Statistical models form an important element in the arsenal of theoretical tools, because they require a minimum of specific assumptions and thus provide useful references against which both data and more detailed theories can be discussed. We recently formulated a statistical model for the calculation of the free energy F associated with an arbitrary specified density distribution $\rho(\mathbf{r})$, held at a constant temperature τ . [1] (The associated statistical weight is then $W_\tau[\rho] = \exp(-F_\tau[\rho]/\tau)$.) This model may form an especially useful basis for addressing the complicated (and yet unknown) configurations occurring in multifragmentation phenomena. The model employs a phenomenological two-body interaction depending both on momentum and density, and it is assumed that the local momentum distribution is of Fermi-Dirac form. In order to ensure that the model be as quantitatively reliable as possible, we chose the interaction so that a broad range of static nuclear properties are reproduced. Specifically, at zero temperature our model is very similar to the Thomas-Fermi model recently developed by Myers and Swiatecki [2] and, therefore, we preserve the very good reproduction they obtain for such important properties as binding energies, matter distributions, and the energy-dependent optical potential. Independently, a rather similar model was recently employed by Bandyopadhyay *et al.* [3] for a range of thermostatic properties of finite and infinite nuclear systems.

However, the broad success of this class of models does not guarantee that their extensions to finite temperature provide accurate descriptions. Therefore, before embarking on quantitative applications to finite-temperature problems, we find it worthwhile to examine carefully the thermostatic properties of the model and ascertain the level of confidence one may have in its results.

Our presentation is organized as follows. First the model developed in ref. [1] is briefly reviewed, for the convenience of the reader, and we describe briefly how thermostatic properties of hot nuclei can be extracted, considering that the nuclei are embedded in a vapor of nucleons, and determine the maximum temperature that such a nucleus can sustain. We then study the level-density parameter a_A , in terms of which the thermal properties of nuclei are often discussed; we derive a useful expansion of A/a_A in powers of $A^{-\frac{1}{3}}$ and give an assessment of the utility of the model at finite temperatures. Subsequently, we derive a liquid-drop expansion of the free energy of a hot nucleus and associated simple analytical approximations.

These results are expected to be useful for discussing a number of aspects associated with the properties of the nuclear systems that may be formed in nuclear collisions at intermediate energies. As a first application to nuclear multifragmentation, we calculate the conditional barriers and associated statistical rates for symmetric breakups of the nucleus ^{120}Sn into various numbers of equal fragments.

2 The model

In our formulation, a system is characterized by its spatial distribution of nucleons, $\rho(\mathbf{r})$, and is assumed to be held at a constant temperature τ . This is different from other treatments, which usually employ a global chemical potential, and has the advantage that any density distribution $\rho(\mathbf{r})$ can be considered, thus making the model applicable to a large class of non-equilibrium configurations. The force between two nucleons is given by the modified Seyler-Blanchard interaction introduced in ref. [1],

$$V_{12}^{\chi} = -C \frac{e^{-r_{12}/a}}{r_{12}/a} \left[1 - \bar{\chi} \frac{p_{12}^2}{b^2} - \chi \frac{\kappa_0}{\rho_0} \left(\left(\frac{\rho_1}{\rho_0} \right)^{\frac{2}{3}} + \left(\frac{\rho_2}{\rho_0} \right)^{\frac{2}{3}} \right) \right]. \quad (1)$$

Here $r_{12} = |\mathbf{r}_1 - \mathbf{r}_2|$ is the spatial separation and $p_{12} = |\mathbf{p}_1 - \mathbf{p}_2|$. Furthermore, ρ_i is short for $\rho(\mathbf{r}_i)$ and the corresponding kinetic density is $\kappa_i = \kappa(\mathbf{r}_i)$. The subscript 0 refers to standard nuclear matter which serves as a convenient reference. The relative strength of the momentum and density dependence is governed by the parameter χ introduced in ref. [1], and its complement $\bar{\chi} = 1 - \chi$, which thus controls the effective mass of the nucleon while leaving the static properties unaffected. For $\chi = 0$ the density-dependence disappears and the original Seyler-Blanchard interaction is recovered. The authors of ref. [3] explore a broader family of interactions by considering several different powers in the density-dependent term. This enables them to consider a range of values of the compressibility modulus K .

As discussed in detail in ref. [2], a good overall reproduction can be obtained for a variety of average nuclear properties with an interaction of the above form, in conjunction with the Thomas-Fermi approximation. In particular, with the value $\chi=0.75$ we obtain a good energy dependence of the optical potential.[1]

The specified density $\rho(\mathbf{r})$ determines a *local* chemical potential $\mu(\mathbf{r})$, and the associated local kinetic-energy density $\kappa(\mathbf{r})$ then follows. Furthermore, a pseudo-kinetic density is defined as $\tilde{\kappa}(\mathbf{r}) = \kappa_0(\rho(\mathbf{r})/\rho_0)^{5/3}$. It is convenient to introduce the following auxiliary functions $\mathcal{R} = Y * \rho$, $\mathcal{K} = Y * \kappa$, and $\tilde{\mathcal{K}} = Y * \tilde{\kappa}$, where the $*$ denotes a convolution with the given Yukawa form factor, $Y(\mathbf{r}) = \exp(-r/a)/r$. In terms of these functions, it is easy to express the effective mass and potential,

$$\frac{m}{B_{\chi}(\mathbf{r})} = 1 + \bar{\chi} \frac{C}{T} \mathcal{R}(\mathbf{r}) \asymp 1 + \bar{\chi} \frac{C}{T} 4\pi a^3 \rho, \quad (2)$$

$$U_{\chi}(\mathbf{r}) = -C \left(\mathcal{R}(\mathbf{r}) - \mathcal{K}_{\text{eff}}(\mathbf{r}) - \frac{5}{3} \chi \frac{\tilde{\kappa}(\mathbf{r})}{\rho(\mathbf{r})} \mathcal{R}(\mathbf{r}) \right), \quad (3)$$

where $\mathcal{K}_{\text{eff}} = Y * \kappa_{\text{eff}}$ with $\kappa_{\text{eff}} = \bar{\chi} \kappa + \chi \tilde{\kappa}$. The second relation for the effective mass holds for uniform matter. Furthermore, the energy and entropy densities are

$$e_{\chi}(\mathbf{r}) = \frac{b^2}{2m} \kappa(\mathbf{r}) - \frac{C}{2} [\mathcal{R}(\mathbf{r})\rho(\mathbf{r}) - \mathcal{K}_{\text{eff}}(\mathbf{r})\rho(\mathbf{r}) - \mathcal{R}(\mathbf{r})\kappa_{\text{eff}}(\mathbf{r})], \quad (4)$$

$$s_{\chi}(\mathbf{r}) = \frac{5}{3} \frac{b^2}{2B(\mathbf{r})\tau} \kappa(\mathbf{r}) - \alpha(\mathbf{r})\rho(\mathbf{r}), \quad (5)$$

where $\alpha(\mathbf{r}) = \beta(\mu(\mathbf{r}) - U(\mathbf{r}))$ is the local fugacity. The free energy of the given system can then be calculated as $F_\tau[\rho] = \int d\mathbf{r}(e_\chi(\mathbf{r}) - \tau s_\chi(\mathbf{r}))$. It is a functional of the specified density $\rho(\mathbf{r})$, as well as a function of the imposed temperature τ . More details can be found in ref. [1].

3 Hot nuclei

In the present work, we consider a variety of nuclear systems embedded in a nucleon vapor held at a constant temperature. The associated selfconsistent density distribution $\rho(\mathbf{r})$ can be decomposed as follows,

$$\rho(\mathbf{r}) = \rho_A(\mathbf{r}) + \rho_V, \quad (6)$$

where ρ_V is the value of the density in the vapor phase and $A = \int d\mathbf{r}\rho_A(\mathbf{r})$ is the nucleon number associated with the embedded ‘‘nucleus’’. It should be noted that the density must attain the value ρ_V away from the nucleus (*i.e.* at a distance large compared with the range of the interaction). The coexistent densities ρ_V and ρ_L are determined uniquely by the temperature τ and can be read off from the associated phase-diagram, see fig. 5 in ref. [1]. To a rough approximation, the phase-coexistence line in the $\rho - \tau$ plane is given by the relationship

$$\frac{\tau}{\tau_c} \approx \left(\frac{\rho}{\rho_c}\right)^{k\frac{\rho_c}{\rho_0}} \left(\frac{\rho_0 - \rho}{\rho_0 - \rho_c}\right)^{k\frac{\rho_0 - \rho_c}{\rho_0}}, \quad (7)$$

where (ρ_c, τ_c) is the critical point and $k \approx 4/5$. Once the temperature $\tau \leq \tau_c$ has been specified, the approximate values of the associated liquid and vapor coexistence densities ρ_L and ρ_V are then the two solutions to the above equation. While the above analytical approximation is somewhat too high at low densities, the difference between the two coexisting densities is very well reproduced by the simple relation

$$\rho_L - \rho_V \approx \rho_0 \left(1 - \frac{\tau}{\tau_c}\right)^{\frac{1}{2}} \left(1 + \frac{1}{2} \frac{\tau}{\tau_c}\right). \quad (8)$$

For a selfconsistent configuration, the chemical potential μ is independent of position. This general feature can be exploited to devise a simple iteration algorithm for obtaining an equilibrium solution to the model: Starting from a suitable approximate distribution having the form of a nucleus embedded in a low-density vapor, we calculate the local chemical potential $\mu(\mathbf{r})$ (see sect. 2); its deviation from the average is then used to improve the local density, and the procedure is repeated until sufficient convergence has been reached. The method can easily be elaborated to ensure that the nucleon number associated with the final embedded nucleus have a specified value.

By means of the decomposition (6), it is possible to extract the thermodynamic quantities associated with the embedded system. For example, the free energy can be obtained as $F_A = F[\rho(\mathbf{r})] - F[\rho_V]$. To appreciate that this prescription is reasonable, it is helpful to imagine that the system is enclosed within an arbitrarily large volume.

The free energy associated with the embedded nucleus is then the free energy of the entire configuration minus the free energy of the same volume filled with the vapor throughout. This procedure is similar to the one suggested by Tubbs and Koonin [4].

3.1 Maximum temperature

It is particularly interesting to calculate the maximum temperature such an embedded hot nucleus can sustain, since this quantity presumably provides an upper bound on the degree of excitation that a compound nucleus can possess. The maximum temperature can be obtained by employing the described iteration algorithm to obtain a selfconsistent solution to the coupled equations in sect. 2, for a specified temperature, and then observing at what temperature it is no longer possible to obtain a modulated solution to the selfconsistent equations, *i.e.* when the only solution is the vapor throughout, $\rho(\mathbf{r}) = \rho_V$.

Figure 1 displays the calculated maximum temperature τ_{\max} as a function of the nuclear mass number A . The dashed curve is drawn to guide the eye, since the calculated values have some numerical error for small mass numbers. For large nuclei τ_{\max} approaches the critical temperature $\tau_c=16.66$ MeV, as it should, and we have found that the calculated τ_{\max} can be well represented by the simple form

$$\tau_{\max} \approx \tau_c - \tau' A^{-\frac{2}{3}}, \quad (9)$$

with $\tau' \approx 67.27$ MeV, for all mass numbers above 25 or so (see fig. 1). This convenient formula is shown in the figure by the dotted curve. We wish to recall that the nuclei considered are isosymmetric and *uncharged*; the addition of the Coulomb repulsion will further reduce the maximum temperature τ_{\max} .

4 Level-density parameter

The thermal properties of a nucleus can be conveniently characterized by its level-density parameter a_A (see, for example, ref. [5]). Calculations of this quantity usually start from the relationship $a_A = (\pi^2/6)g_A$, where g_A is the density of single-particle states at the Fermi surface. This latter quantity can be calculated by semi-classical means. Thus, employing the Thomas-Fermi approximation, we observe that the number of single-particle states with energy less than a specified value ϵ is given by

$$N(\epsilon) = g \int \frac{d\mathbf{r}d\mathbf{p}}{h^3} \theta(h(\mathbf{r}, \mathbf{p}) - \epsilon), \quad (10)$$

where $g=4$ is the spin-isospin degeneracy and $h(\mathbf{r}, \mathbf{p})$ is the effective single-particle hamiltonian. For the modified Seyler-Blanchard interaction (1), this latter quantity is of standard form, $h(\mathbf{r}, \mathbf{p}) = p^2/2B(\mathbf{r}) + U(\mathbf{r})$, with $B(\mathbf{r})$ and $U(\mathbf{r})$ given in eqs. (2) and (3), respectively. It is then possible to carry out the momentum integral in the above expression for $N(\epsilon)$, and a subsequent differentiation then yields the result

$$a_A = \frac{\pi^2}{6} \left(\frac{dN(\epsilon)}{d\epsilon} \right)_{\epsilon=\mu} = \frac{\pi}{3} \frac{g}{\hbar^3} \int_0^{r>} r^2 dr [2B(r)(\mu - U(r))]^{\frac{1}{2}} B(r), \quad (11)$$

where the condition $U(r_>) = \mu$ determines the upper bound on the integration.

An alternative method for obtaining the level-density parameter is to employ the relation

$$a_A = \frac{1}{2} \frac{dS_A}{d\tau}, \quad (12)$$

where $S_A = S[\rho] - S[\rho_V]$ is the entropy of the embedded nucleus. The entropy density can be expressed as $s(\mathbf{r}) = [\frac{5}{3}F_{\frac{3}{2}}(\alpha) - \alpha F_{\frac{1}{2}}(\alpha)]\rho_\tau(\mathbf{r})$, where $\alpha(\mathbf{r})$ is the local fugacity and $F_n(\alpha)$ are the usual Fermi integrals (see ref. [1]). We then find

$$\frac{ds}{d\tau} \approx \frac{1}{\tau} [\frac{5}{2}F_{\frac{3}{2}}(\alpha(\mathbf{r})) - 3\alpha F_{\frac{1}{2}}(\alpha(\mathbf{r})) + \frac{1}{2}\alpha(\mathbf{r})^2 F_{-\frac{1}{2}}(\alpha(\mathbf{r}))]\rho_\tau(\mathbf{r}), \quad (13)$$

neglecting the temperature variation of the effective hamiltonian $h(\mathbf{r}, \mathbf{p})$. The above expression is exact at zero temperature, but when τ is finite there are small corrections arising from the temperature dependence of the mean field $U(\mathbf{r})$. Once the selfconsistent solution is determined, the above expression (13) for the derivative of the entropy density can readily be evaluated and the level-density parameter can be obtained by integrating over the domain of the nucleus.

We have verified that the two above methods indeed yield the same numerical results, at zero temperature. At finite temperatures the elementary relation $a_A = (\pi^2/6)g_A$ is no longer valid and the first method (11) can no longer be used, whereas the expression (12) applies at any temperature (although the approximation (13) is not fully accurate at finite temperatures). However, rather than employing this latter method, it is more convenient to consider the *effective* level-density parameter $a_A^{\text{eff}} = E^*/\tau^2$, since this quantity can be obtained directly from the excitation energy of the nucleus, E^* .

Because a_A is approximately proportional to the mass number A , it is useful to write the nuclear level-density parameter on the form $a_A = A/\varepsilon_A$. The characteristic energy ε_A then depends only relatively slightly on the size and shape of the system. For the calculations, it is more convenient to consider its inverse, the *reduced* level-density parameter $\tilde{a} = a_A/A = 1/\varepsilon_A$.

4.1 Nuclear matter

Let us first consider uniform nuclear matter, in which the density distribution is constant. In this simple case the reduced level-density parameter is

$$\tilde{a}_{\text{bulk}} = \left(\frac{g}{\pi^2} \frac{m}{B} \frac{P_F^2}{2m} \right)^{-1}. \quad (14)$$

Thus \tilde{a}_{bulk} depends on the density ρ through both the Fermi kinetic energy $P_F^2/2m \sim \rho^{2/3}$ and the effective mass B given by (2). With the parameter values adopted in ref. [1], the equilibrium density of symmetric nuclear matter is $\rho_0 \approx 0.153 \text{ fm}^{-3}$, and so the associated effective mass is $B \approx 0.71 m$. It then follows that the level-density parameter for standard nuclear matter is $\tilde{a}_0 = (20.384 \text{ MeV})^{-1}$. We note that the value of \tilde{a}_0 is decreased by the factor $B/m \approx 0.71$ arising from the effective mass of the nucleon in the nuclear matter.

When the specified constant density ρ deviates only little from the saturation value ρ_0 (*i.e.* when $\Delta\rho = \rho - \rho_0 \ll \rho_0$), a Taylor expansion is accurate,

$$\tilde{a}_{\text{bulk}} \approx \tilde{a}_0 + (\rho - \rho_0) \left(\frac{\partial \tilde{a}}{\partial \rho} \right)_{\rho_0} = \tilde{a}_0 \left(1 - \frac{2 \Delta\rho}{3 \rho_0} \frac{1 + \frac{5}{2} \bar{\chi} \frac{C}{T} \mathcal{R}_0}{1 + \bar{\chi} \frac{C}{T} \mathcal{R}_0} \right). \quad (15)$$

This result is useful when finite nuclei are considered, because the nuclear surface tension acts to compress the nucleus somewhat, thus enhancing its bulk density.[6]

A simple but quantitatively accurate expression for this effect can be obtained by exploiting the leptodermous character of nuclei, which allows the nuclear energy to be split into bulk and surface terms.[6] Thus, for a spherical nucleus of radius R , we may write

$$E(A, R) = A\epsilon_{\text{bulk}} + 4\pi R^2 \gamma_0. \quad (16)$$

Here ϵ_{bulk} is the energy per nucleon in uniform matter (having a density equal to that in the bulk of the nucleus) and γ_0 is the nuclear surface tension at zero temperature. Furthermore, the nuclear radius R is related to the bulk density ρ by $(4\pi/3)R^3\rho = A$, with A being the nucleon number of the nucleus. The energy per nucleon for bulk matter ϵ_{bulk} can be written in terms of the compressibility modulus K as

$$\epsilon_{\text{bulk}} = \epsilon_0 + \frac{K}{2} \left(\frac{R - R_0}{R_0} \right)^2, \quad (17)$$

where ϵ_0 is the energy per nucleon in standard nuclear matter and $R_0 = r_0 A^{1/3}$ with $(4\pi/3)r_0^3\rho_0 = 1$. By minimizing the above energy expression with respect to the radius R , it is possible to determine the bulk compression of a spherical nucleus in its ground state,

$$\frac{\Delta\rho}{\rho_0} = \frac{6a_2}{K} A^{-\frac{1}{3}} = 0.355 A^{-\frac{1}{3}}, \quad (18)$$

where $K = 305.0$ MeV is the compressibility coefficient [1] and $a_2 = 4\pi r_0^2 \gamma_0 = 18.06$ MeV is the usual surface energy coefficient (see below).

Using this result for the nuclear compression in conjunction with (15), the bulk contribution to the nuclear level-density parameter can be written as follows,

$$\tilde{a}_A^{\text{bulk}} = \tilde{a}_0 \left(1 - \frac{4a_2}{K} \frac{1 + \frac{5}{2} \bar{\chi} \frac{C}{T} \mathcal{R}_0}{1 + \bar{\chi} \frac{C}{T} \mathcal{R}_0} A^{-\frac{1}{3}} + \dots \right) \approx \tilde{a}_0 (1 - 0.339 A^{-\frac{1}{3}}). \quad (19)$$

4.2 Nuclear slab

To determine the surface contribution to the level density, it is useful to consider a nuclear slab, whose density varies only in one direction, while there is translational symmetry in the transverse plane. Because of the flat geometry, a compression would not reduce the surface area and, consequently, the bulk density of the slab is not enhanced relative to that of standard nuclear matter ρ_0 . For notational convenience, we use R to denote half the width of the slab and also introduce the quantity $\tilde{A} = (4\pi/3)R^3\rho_0$, *i.e.* the nucleon number of a spherical nucleus with the same diameter (and the same bulk density) as the slab.

The energy per nucleon for a slab in equilibrium can then be written

$$\epsilon_{\text{slab}} = \epsilon_0 + a_2 \tilde{A}^{-\frac{1}{3}} . \quad (20)$$

The surface energy coefficient a_2 can then be determined from the behavior of the energy as the width of the slab grows large. Considering the range $R=4-15$ fm, we find the value $a_2 = 18.06$ MeV employed above, using the parameter values of ref. [1].

A similar expansion holds for the reduced level-density parameter,

$$\tilde{a}_{\text{slab}} = \tilde{a}_0(1 + c_2^0 \tilde{A}^{-\frac{1}{3}}) , \quad (21)$$

and the associated surface coefficient c_2^0 can be determined in a similar manner, by considering \tilde{a} for large values of R . Fitting to values of \tilde{A} calculated for slab widths in the same R range, we obtain $c_2^0 = 0.7117$.

This result may be compared with the estimates made by Töke and Swiatecki[7]. Transcribing their results to our present notation, we get $c_2^{TS} = 3.114/F_2 = 1.038$, since the geometric coefficient F_2 has the value 3 for the slab. In view of the considerable differences between the two calculations (for example, ours is selfconsistent and employs an effective mass), the rough agreement is gratifying. It is noteworthy that the ratio of the two results for c_2 is very similar to the corresponding ratio between the bulk values \tilde{a}_0 , namely the relative value of the effective mass, $B/m \approx 0.71$.

4.3 Nuclear sphere

Let us now turn to spherical nuclei. Because of the leptodermous character of nuclei, it is useful to express the reduced level-density parameter \tilde{a}_A as a series in powers of $A^{-1/3}$. The leading term is \tilde{a}_0 , the reduced level-density parameter for standard nuclear matter. There are two contributions to the first-order correction, one arising from the compressed interior and another associated with the surface. We may therefore write

$$\tilde{a}_A = \tilde{a}_0(1 + c_2 A^{-\frac{1}{3}} + c_3 A^{-\frac{2}{3}} + \dots) . \quad (22)$$

Here the coefficient of the leading correction term is given by

$$c_2 = F_2^{\text{slab}} c_2^0 - \frac{4a_2}{K} \frac{1 + \frac{5}{2} \bar{\chi}_T^C \mathcal{R}_0}{1 + \bar{\chi}_T^C \mathcal{R}_0} = 1.7958 . \quad (23)$$

The first term is associated with the nuclear surface while the second term in c_2 (which is smaller by an order of magnitude) arises from the bulk compression (see eq. (19)). The coefficient F_2 denotes the ratio between the actual surface area and that of the equivalent sphere.[7] For a slab, this quantity is readily found to be equal to 3, as already used above.

The second-order correction coefficient c_3 can be determined by considering the behavior of \tilde{a}_A for large spherical nuclei. Fitting the expression (22) for nuclei with radii in the range $R = 4-15$ fm we obtain $c_3 = 0.0665$. Thus, in summary, we find the following leptodermous expansion for the reduced nuclear level-density parameter,

$$\tilde{a}_A = \frac{a_A}{A} = \frac{1}{20.384 \text{ MeV}} (1 + 1.796 A^{-\frac{1}{3}} + 0.066 A^{-\frac{2}{3}} + \dots) . \quad (24)$$

Because of the smallness of c_3 , the last term is practically unimportant. Figure 2 shows the calculated values of $\varepsilon_A = A/a_A$ as a function of A (solid points) together with the derived leptodermous expansion (24). It is seen that the expression (24) gives a quite good reproduction of the calculated values for finite nuclei.

It should be noted that a leptodermous expansion is asymptotic in character and so is expected to become accurate in the limit of large A . For small values of A its accuracy cannot necessarily be improved by going to higher order in $A^{-1/3}$. Indeed, when the size of the system is comparable to the range of the interaction, finite-range contributions are significant and these cannot be subjected to such an expansion. As a consequence of this feature, a leptodermous expansion may be somewhat inaccurate for actual nuclei for which the radius is not much larger than the range of the nuclear force. However, since the coefficient c_3 in (24) has been fitted to finite nuclei, rather than determined by bending slabs, it takes partial account of the finite-size effect and the resulting expression is in fact rather accurate for ordinary nuclei (see fig. 2).

In order to provide an optimally accurate formula, one may adjust all the three parameters of the expression (24) so as to achieve a reproduction of the calculated level-density parameter a_A through the mass region $A=25$ -250. Such a three-parameter fit yields the following result,

$$\frac{a_A}{A} \approx \frac{1}{20.17 \text{ MeV}} (1 + 1.604A^{-\frac{1}{3}} + 0.976A^{-\frac{2}{3}}). \quad (25)$$

We notice that the leading term is close to the bulk value 20.384 MeV, and the coefficient of the first correction term is not much different from the idealized result in (24). However, the coefficient of the second correction term is larger than c_3 in (24) by more than one order of magnitude. The results of this fitted expression (25) are also included in fig. 2 and gives a nearly perfect reproduction of the calculated values. This relation may therefore be used with confidence.

4.4 Discussion

In the preceding, we have derived a leptodermous expansion for the level-density parameter for macroscopic nuclei at zero temperature. It is interesting to compare our result with that obtained by Tōke and Swiatecki [7] using idealized density distributions. The most significant difference arises from the fact that we have an effective mass, due to the momentum dependence of the Seyler-Blanchard interaction (1). The leading term, associated with the nuclear bulk, is then correspondingly enhanced by the factor $m/B \approx 1.4$. A similar enhancement was found for the coefficient c_2 of the first correction term, so that the relative size of the first-order correction in $A^{-1/3}$ comes out very similar to the result of ref. [7]. However, the coefficient c_3 associated with the second-order correction is nearly two orders of magnitude smaller than the corresponding one obtained in ref. [7]. We suspect that this difference arises in large part because the results, at this level of accuracy, have a high sensitivity to the model details, especially the density profile. This feature has long marred attempts to calculate the nuclear curvature energy.

When applied to medium-heavy and heavy nuclei, our present model calculations yield typical values of $\varepsilon_A = A/a_A \approx 15$ -17 MeV. By contrast, the experimental values

of the inverse of the reduced level-density parameter are $\varepsilon_A^{\text{exp}} \approx 8\text{-}10$ MeV, as obtained from analysis of neutron-absorption data.[5] Thus, the calculation overestimates ε_A by roughly 50%, which is about the size of m/B . This is a well-known shortcoming of mean-field calculations and numerous investigations have demonstrated that the inclusion of correlations help to bring ε_A down into better agreement with the data.

When judging this discrepancy, it should be remembered that the experimentally explored excitation energies are given approximately by the neutron separation energy, *i.e.* ≈ 8 MeV, which is relatively small compared to the total binding energy, and at such low excitations there are significant contributions to the level density from a variety of collective modes, thus increasing a_A considerably. However, as the temperature is raised above a few MeV, the collective modes have largely dissipated and a calculation treating only the single-particle degrees of freedom should grow more appropriate.

Such an expected increase of ε_A with temperature is indeed observed experimentally and can, to a large degree, be understood theoretically, as discussed recently by Shlomo and Natowitz [8], for example. By taking approximate account of the long-range (*RPA*) correlations by introducing a frequency-dependent effective mass, they find a gradual increase of ε_A from around 8 MeV at zero temperature towards 15-17 MeV for $\tau = 8\text{-}10$ MeV. Moreover, this behavior is in reasonable (though not perfect) agreement with the extracted experimental values. These results are shown in fig. 3. It is seen that indeed, at high temperatures, our present calculation agrees fairly well with the calculation of ref. [8], which in turn accounts well for the trends of the data.

Thus, in conclusion, the present model significantly underestimates the level-density parameter a_A at low temperatures, by roughly 70%, although a reasonable behavior is obtained for temperatures above 5 MeV, or so (see fig. 3). This is a well-known problem common to mean-field approaches and thus not easily remedied by adjustments in the interaction. Application to finite temperatures must therefore be made with caution and the results should not be regarded as quantitatively reliable, unless the temperature is sufficiently high. Clearly, there is a need for augmenting this class of models, so as to account realistically for the specific heat of nuclear systems, without spoiling their simplicity and overall good agreement with a wide body of other nuclear properties, including the energy dependence of the optical potential.

5 Free energy

With the method described above, it is straightforward to derive a liquid-drop formula for the free energy of a hot nucleus. Our goal here is to obtain a simple expression for the free energy of an arbitrary nucleus in equilibrium with a surrounding vapor at a finite temperature. This is important because, once the free energy is known, the associated statistical weight can be immediately obtained as $W = \exp(-F[\rho]/\tau)$. Considering the volume and surface terms only, we may write

$$F_A(\tau) = -a_1(\tau)A + a_2(\tau)A^{2/3}, \quad (26)$$

where a_1 and a_2 are the volume and surface coefficients, respectively. At zero temperature, a_1 reduces to the value 16.037 MeV associated with cold nuclear matter, and a_2 becomes the usual surface energy coefficient used above, $a_2(0) = 18.06$ MeV.

To find the temperature dependences of a_1 and a_2 , we start by writing F_A as

$$F_A(\tau) = A (\phi[\rho_A(\mathbf{r}, \tau) + \rho_V(\tau)] - \phi[\rho_V(\tau)]) + 4\pi R(\tau)^2 \gamma(\tau). \quad (27)$$

Here $\rho_A(\mathbf{r}) + \rho_V$ is the selfconsistent solution and $\phi[\rho]$ denotes the average free energy per nucleon of the specified density distribution, as obtained on the basis of the corresponding free-energy density. It should be noted that in the limit of very large nuclei the situation is similar to that of uniform nuclear matter, and so the central density $\rho_A^0(\tau) + \rho_V(\tau)$ approaches the value $\rho_L(\tau)$ associated with the liquid phase coexisting with the vapor density $\rho_V(\tau)$ at the temperature τ (see fig. 5b of ref. [1]). In such a case, the bulk value of the nuclear free energy can be written as

$$F_A^0(\tau) = \frac{\rho_L(\tau)\phi_L(\tau) - \rho_V(\tau)\phi_V(\tau)}{\rho_L(\tau) - \rho_V(\tau)} A. \quad (28)$$

For finite nuclei the compressional effect discussed in sect. 4.1 causes the bulk value of the nuclear density to be increased by the amount $\Delta\rho = \rho_A + \rho_V - \rho_L$. The corresponding expression for F_A is then

$$F_A(\tau) = F_A^0(\tau) + \frac{K}{18} \left(\frac{\Delta\rho}{\rho_A^0}\right)^2 A + 4\pi R_A^{02} \left(1 - \frac{1}{3} \frac{\Delta\rho}{\rho_A^0}\right)^2 \gamma(\tau). \quad (29)$$

Here R_A^0 is the radius of the non-compressed density distribution ($\rho_A^0 = \rho_L - \rho_V$) of the embedded nucleus. By minimizing the expression above with respect to the density we obtain

$$\frac{\Delta\rho}{\rho_A^0} \approx \frac{6\gamma}{K} \frac{3}{R_A^0 \rho_A^0}, \quad (30)$$

which is analogous to (18). Therefore, the leading term of the contribution from the compression to the free energy of the nucleus is proportional to $A^{1/3}$ and hence is important only for small nuclei. If we retain terms in A and in $A^{2/3}$ only, and define the temperature-dependent effective radius constant $r_0(\tau)$ through the condition $(\rho_L(\tau) - \rho_V(\tau))4\pi r_0(\tau)^3/3 = 1$, we may rewrite eq. (29) as

$$\phi_A(\tau) = \frac{\rho_L\phi_L - \rho_V\phi_V}{\rho_L - \rho_V} + \frac{3\gamma(\tau)}{\rho_L - \rho_V} \frac{1}{R_A^0}, \quad (31)$$

where we have used that $R_A^0(\tau) = r_0(\tau)A^{1/3}$. The denominator, $\rho_L(\tau) - \rho_V(\tau)$, is obtained from the coexistence curve in the phase diagram of nuclear matter and is given to a good approximation by eq. (8). The free energies per nucleon, ϕ_L and ϕ_V , are those associated with the respective coexisting liquid and vapor phases.

Thus, the volume coefficient for the free energy is easily obtained as

$$a_1(\tau) = -\frac{\rho_L\phi_L - \rho_V\phi_V}{\rho_L - \rho_V}. \quad (32)$$

Figure 5 shows the resulting a_1 as a function of τ (solid circles). These values are well reproduced by the following simple expression,

$$a_1(\tau) \approx a_1(0) + \tilde{a}_0 \tau^2 \left(1 - \frac{1}{16} \left(\frac{\tau}{\tau_c}\right)^2\right), \quad (33)$$

where $a_1(0) = 16.037$ MeV is the volume coefficient at $\tau = 0$, and $\tilde{a}_0 = 1/(20.384$ MeV) is the bulk term in the leptodermous expansion of the level-density parameter (24).

Eq. (31) has been derived for a spherical geometry. The formula for a slab is very similar, except for the fact that there is no factor 3 (see sect. 4.2). Besides, as the bulk density of the slab is not enhanced relative to that of uniform nuclear matter, the resulting expression for the free energy per nucleon,

$$\phi_A^{\text{slab}}(\tau) = \frac{\rho_L \phi_L - \rho_V \phi_V}{\rho_L - \rho_V} + \frac{\gamma(\tau)}{\rho_L - \rho_V} \frac{1}{R_A^0}, \quad (34)$$

is more accurate than eq. (31). (We recall that we are considering a slab with the same bulk density as a nucleus whose diameter is equal to the width of the slab). Thus, for each temperature, the value of γ is obtained from the behavior of ϕ^{slab} as the width $2R$ increases. The values of γ thus obtained are shown in fig. 4 as a function of the temperature. As is evident, our calculations (solid circles) are very well reproduced by the formula

$$\gamma(\tau) \approx \gamma_0 \left(1 + \frac{3}{2} \frac{\tau}{\tau_c}\right) \left(1 - \frac{\tau}{\tau_c}\right)^{\frac{3}{2}}, \quad (35)$$

where $\gamma_0 = 1.069$ MeV/fm² is the standard surface tension and the critical temperature is $\tau_c = 16.66$ MeV [1]. This analytical form was first suggested by Goodman, Kapusta and Mekjian [9], and it has been employed in a variety of studies since then but has not actually been tested for accuracy, as far as we are aware. Our present results demonstrate that this expression is indeed a very good representation of the calculated behavior.

To obtain the surface energy coefficient $a_2(\tau)$ entering into the liquid-drop formula (26), we note that

$$a_2(\tau) = \frac{(36\pi)^{1/3} \gamma(\tau)}{(\rho_L(\tau) - \rho_V(\tau))^{2/3}} \approx a_2(0) \left(1 + \frac{3}{2} \frac{\tau}{\tau_c}\right) \frac{\left(1 - \frac{\tau}{\tau_c}\right)^{7/6}}{\left(1 + \frac{1}{2} \frac{\tau}{\tau_c}\right)^{2/3}}, \quad (36)$$

where we have used the approximation (8) and the relationship $a_2(\tau) = 4\pi r_0(\tau)^2 \gamma(\tau)$. For $\tau = 0$ the vapor density vanishes so $\rho_L - \rho_V$ equals the saturation density ρ_0 . The denominator in eq. (36) is a monotonically decreasing function of the temperature and it vanishes at $\tau = \tau_c$ as $\rho_L - \rho_V \sim (\tau_c - \tau)^{1/2}$, so that the radius constant diverges as $r_0 \sim (\tau_c - \tau)^{-1/6}$. Nevertheless, since the surface tension by itself vanishes as $\gamma \sim (\tau_c - \tau)^{3/2}$, the surface-energy coefficient tends to zero as it should, $a_2 \sim (\tau_c - \tau)^{7/6}$ (there is no surface tension at the critical point).

The calculated values of the surface coefficient $a_2(\tau)$ are included in fig. 5, together with the above analytical formula (36). We note that the approximations to $a_1(\tau)$ and $a_2(\tau)$ are excellent for all temperatures.

The liquid-drop formula derived above is valid at any temperature below τ_c and is applicable for all mass numbers, provided a selfconsistent solution for the density distribution can be found at the temperature specified. However, in view of the discussion at the end of sect. 4, we expect the result to be more realistic for systems that are not too cold.

6 Multifragmentation

We conclude this presentation by making a first application to nuclear multifragmentation, the (so far hypothetical) process by which an excited system breaks up into several nuclear fragments nearly simultaneously. We build here on the formulation developed by López and Randrup [10], who have generalized the Bohr-Wheeler treatment to the spontaneous transformation of a source into an assembly prefragments. For the purpose of being able to study arbitrary density distributions, we have made a three-dimensional implementation of the model, in which the density (and all other local quantities) are given on a grid. The illustration below has been calculated with this general code, although the very special configurations considered might well make the problem tractable by simpler numerical methods.

We shall parametrize each manifestation of the system as an assembly of N spherical fragments, situated at the positions $\{\mathbf{r}_n\}$. The matter density distribution of each fragment is obtained by convoluting a sharp generating sphere with a Yukawa function. Its range $a_\rho = 1/\sqrt{2}$ fm is chosen so that the diffuseness of a flat surface is $b=1$ fm. The radius of the generating sphere is $R_n = r_0 A_n^{1/3}$, with $3/(4\pi r_0^3) = \rho_0 = 0.153 \text{ fm}^{-3}$ (implying $r_0 \approx 1.16$ fm). The resulting matter distribution $\rho(\mathbf{r})$ is subject to the modified Seyler-Blanchard interaction (1), as well as the Coulomb force. The energy $E[\rho]$ can then be calculated by using the formalism developed in ref. [1], augmented by the standard Coulomb integral (which requires the major part of the computational effort).

It is instructive to consider the breakup into fragments of equal size and arranged in a spatially symmetrical manner. It is then convenient to use the nucleus ^{120}Sn as the source, and we assume that the total charge of 50 elementary units is distributed evenly among all the 120 nucleons, irrespective of the particular configuration considered. Thus, the binary channel is parametrized as two fragments with mass numbers $A_1 = A_2 = 60$ at a specified separation, the ternary configurations have three fragments of mass 40 arranged in an equilateral triangle, and the quaternary configurations are tetrahedric positionings of four mass-30 fragments. For $N = 6$ we position the fragments at equal distances along the positive and negative directions of three cartesian directions, and for $N = 8$ the fragments are positioned in the corners of a cube. The highest multiplicity considered has $N = 12$ and the fragments are situated in a dodekahedric configuration, *i.e.* in the centers of twelve pentagons that have been fit together in a closed surface approximating a sphere. As an alternative 12-fragment configuration, we position the fragments on the centers of the edges of a cube (this leads to a somewhat less symmetric appearance, although all the fragments are still entirely equivalent).

It is convenient to characterize the fragmenting system in a parametrization-independent manner in terms of its root-mean-square extent q , where

$$q^2 \int d\mathbf{r} \rho(\mathbf{r}) = \int d\mathbf{r} r^2 \rho(\mathbf{r}) = \sum_{n=1}^N A_n (r_n^2 + \frac{3}{5} R_n^2 + 6a_\rho^2). \quad (37)$$

For each of the special multifragment arrangements described above, we then calculate the energy of the system as a function of the size q , keeping the temperature at zero. This procedure leads to a conditional potential energy of deformation $V_{1\dots N}(q)$ for each particular channel. The results are shown in fig. 6. Of course, since we use a restricted parametrization, the results are correspondingly approximate. The description in terms of N spherical fragments is most relevant at large separations, while these special configurations become increasingly disfavored for more compact configurations (*i.e.* smaller values of q), where energy can be gained by fragment distortions and, subsequently, neck formation. In particular, the barrier calculated for the disphere is expected to significantly exceed the actual symmetric-fission barrier, and the more so the heavier the system is (since the barrier shape is then more compact). To give a feeling for the domain of utility, the points at which the generating sharp spheres touch are shown by the vertical bars. For more compact configurations the generating spheres partially overlap and the energy starts to increase, reflecting the cost associated with doubling the nuclear density. However, in spite of its obvious limitations, the multisphere parametrization is useful, both for bringing out the qualitative features and for allowing approximate quantitative calculations.

We observe that the barrier tops grow systematically higher with the fragment multiplicity N , as would be expected because of the increased surface-to-volume ratio. At the same time the location of the top moves out to larger values of q , as is characteristic of systems fragmenting into smaller parts. We note, in particular, that the barrier tops are situated well outside the point at which the corresponding generating sharp spheres touch, except perhaps for the binary channel. We also note that the two different spatial arrangements for $N=12$ produce rather similar conditional potential barriers. Figure 6 also shows the potential energy associated with a monopole distortion of the ^{120}Sn source nucleus. This parabola-like curve can be approximately constructed on the basis of the nuclear compressibility modulus $K=305$ MeV.

As shown in ref. [10], the statistical weight of a multifragment configuration is a product of a macroscopic factor resulting from the translational motion of the individual fragments and a microscopic factor expressing the internal excitations in the fragments. The energy available for fragment motion and internal excitation is given by $\epsilon_{1\dots N} = E - V(q_{1\dots N})$, where E is the specified total energy of the system and V is the calculated potential energy associated with the considered configuration. This quantity is also the maximum internal excitation energy that the system can have (corresponding to all fragments being at rest). The corresponding maximum internal temperature $\tau_{1\dots N}$ has been calculated from the approximate relation $\epsilon_{1\dots N}/N = a_n \tau_{1\dots N}^2$, using the level-density parameter (25) associated with the mass number of the fragment, $A_n = A/N$. Since this energy is generally shared statistically between the internal excitations and the translational motion of the individual

fragments, the internal excitation is distributed around a somewhat smaller value $\bar{\epsilon}$, with a corresponding most probable temperature given by

$$\bar{\tau} = \tau_{1\dots N}[(1 + \xi^2)^{\frac{1}{2}} - \xi], \quad \xi = \frac{3N - 4}{2} \frac{\tau_{1\dots N}}{2\epsilon_{1\dots N}}. \quad (38)$$

Under the assumption of statistical equilibrium, the outwards directed statistical current can be written on the form[10]

$$\nu_{A_1\dots A_N}(E) = \frac{1}{h} \frac{\sqrt{4\pi}}{\Gamma(\frac{3}{2}N - \frac{3}{2})} \left(\frac{mAq_{1\dots N}^2 \bar{\tau}}{2\hbar^2} \right)^{\frac{3}{2}N-2} \rho_{1\dots N}(\epsilon_{1\dots N}) \bar{\tau}, \quad (39)$$

calculated near the top of the barrier where it attains its minimum value, and the partial width associated with a statistical disassembly into a particular multifragment channel is $\Gamma_{A_1\dots A_N} = h\nu_{A_1\dots A_N}/\rho(A, E)$, where the denominator is the total density of states of the source, including its many different multifragment partitions. Since this latter quantity is not readily calculable, we consider the relative partial widths, or branching ratios, $\Gamma_{A_1\dots A_N}/\Gamma_{A_1A_2} = \nu_{A_1\dots A_N}/\nu_{A_1A_2}$.

These quantities are displayed in fig. 7. There are two opposing effects determining these results: 1) as the fragment multiplicity N is increased, more surface area needs to be created and, therefore, the barrier grows higher and the energy available for statistical excitation decreases; 2) the statistical weight arising from the fragment motion increases, because the associated power is linear in N . As a consequence of this interplay, the binary channel is favored at low energies, where the barrier increase is the decisive effect, whereas the multifragment channels dominate at high excitation, where the macroscopic phase-space is overwhelming. Generally, the slope of the curve increases with the multiplicity N . The binary curve is then overtaken by the ternary curve at around 4 MeV per nucleon, this curve is in turn overtaken by the quaternary curve at around 4.5 MeV per nucleon, and so on, with $N=12$ becoming the dominant mode at around 6 MeV per nucleon.

It should be kept in mind that the displayed results pertain to one specific multifragment mass partition for each value of N considered, and for each of these only one (especially symmetric) arrangement has been considered (except for $N=12$ where an alternative symmetric arrangement has also been explored). There are many distinct mass partitions for each multiplicity N , and the more so, the larger N is. This feature enhances the combined relative weight of fragmentations with a large multiplicity. Figure 7 therefore suggests that the change from binary to multifragment dominance occurs within a relatively narrow energy range around 4 MeV per nucleon.

Finally, we emphasize that the present calculation should be regarded as somewhat schematic, because of the restricted shape parametrizations. A more complete exploration of the configuration space would lower the conditional barriers somewhat, especially for $N=2$. Our exploratory calculations indicate that such a lowering of the fission barrier would reduce the branching ratios somewhat, thereby moving the curves upwards in energy by perhaps one MeV, but the general pattern would remain.

7 Concluding remarks

In the present work, we have employed the model developed in ref. [1] for a study of the thermostatic properties of nuclei, for the dual purposes of deriving simple useful formulas and assessing the quantitative utility of the model.

First, we calculated the maximum temperature that a hot nucleus embedded in a vapor can sustain and found a steady increase from essentially $\tau = 0$ for the smallest nuclei to $\tau \approx \tau_c$ for very large (uncharged) systems. We then made a systematic derivation of a leptodermous expansion for the level-density parameter and also determined its dependence on temperature. A similar treatment was made for the free energy of a hot nucleus, a key quantity in determining the statistical weight of a multifragment configuration. Along with the numerical calculations, we determined quantitatively accurate analytical approximations for the mass and temperature dependence of the quantities considered: the level-density parameter a_A , the surface tension γ , and the volume and surface coefficients a_1 and a_2 in the liquid-drop formula for the free energy F_A . These simple formulas may be of practical utility in a variety of contexts, since their applicability is not expected to depend much on the specifics of the model, provided that the appropriate characteristic quantities, such as saturation density and critical temperature, are properly replaced.

In our discussion, we pointed out that the level-density parameter implied by the modified Seyler-Blanchard model is significantly smaller than the experimentally extracted values, a problem common to this type of model. Therefore, the thermostatic predictions of these models are inaccurate at low temperatures and appropriate caution should therefore be exercised. On the other hand, for temperatures above 5 MeV, or so, the model appears to yield quite reasonable results, agreeing with both more refined theoretical calculations and the values extracted from experiment. Since our primary goal has been to develop a model that can be brought to bear on multifragmentation problems, we have some confidence in the model, in so far as the relevant temperatures are expected to be at least several MeV.

This fact is illustrated by our schematic application of the model to the multifragment breakup of ^{120}Sn . Using a general three-dimensional computer code, we first calculated the conditional potential-energy barriers associated with the symmetric breakup into a number of equal fragments and then obtained the corresponding relative partial breakup widths, using the statistical treatment developed in ref. [10]. The behavior of these widths with excitation energy suggests that the preferential disassembly mode changes relatively rapidly from fission-like binary splits to multifragment breakup in the vicinity of 4 MeV per nucleon. We therefore expect that the developed model will be useful for discussing a number of aspects associated with the disassembly of highly excited nuclear systems that may be formed in nuclear collisions at intermediate energies.

This work was supported in part by the Director, Office of Energy Research, Division of Nuclear Physics of the Office of High Energy and Nuclear Physics of the U.S. Department of Energy under Contract No. DE-AC03-76SF00098. We also wish to acknowledge useful discussions with W.D. Myers and W.J. Swiatecki. One of us (ELM) would like to express his gratitude to the Nuclear Theory Group at the LBL for the kind hospitality.

References

- [1] J. Randrup and E. de Lima Medeiros, LBL-28797: Nucl. Phys. A (1991) in press
- [2] W.D. Myers and W.J. Swiatecki, Ann. Phys. 204 (1990) 401; LBL-30395: Ann. Phys. (1991) in press
- [3] D. Bandyopadhyay, C. Samanta, S.K. Sammaddar, and J.N. De, Nucl. Phys. A511 (1990) 1
- [4] D.L. Tubbs and S.E. Koonin, Astrophys. J. 232 (1979) L59
- [5] A. Bohr and B.R. Mottelson, *Nuclear Structure 1*, (Benjamin, New York, 1969)
- [6] W.D. Myers and W.J. Swiatecki, Ann. Phys. 55 (1969) 395
- [7] J. Tōke and W.J. Swiatecki, Nucl. Phys. A372 (1981) 141
- [8] S. Shlomo and J.B. Natowitz, Phys. Lett. 252B (1990) 187
- [9] A.L. Goodman, J.I. Kapusta, and A.Z. Mekjian, Phys. Rev. C30 (1984) 851
- [10] J.A. López and J. Randrup, Nucl. Phys. A503 (1989) 183

Figure 1: Maximum temperature

The calculated maximum temperature τ_{\max} for which an embedded excited nucleus of specified mass number A can exist. The dotted curve shows the simple asymptotic approximation (9), while the dashed curve serves to guide the eye.

Figure 2: Level-density parameter

The quantity A/a_A associated with spherical nuclei is plotted as a function of the mass number A . The solid points show the calculated values for specific values of the nucleon number A . The leptodermous expansion (24) is shown by the solid curve, while the dashed curve represents the fitted expression (25).

Figure 3: Temperature dependence

The inverse of the effective reduced level-density parameter, $A/a_A^{\text{eff}} = \tau^2/\epsilon^* = \epsilon^{\text{eff}}$ as a function of the temperature τ , for an uncharged isosymmetric nucleus with mass number $A = 160$. The solid curve represents our calculated results, while the dashed curve is the result obtained in ref. [8] by including a frequency-dependent effective mass. Both this curve and the data points are taken from fig. 2 of that paper.

Figure 4: Surface tension

The temperature dependence of the surface tension $\gamma(\tau)$ as calculated on the basis of eq. (34), together with the analytical approximation (35).

Figure 5: Free energy

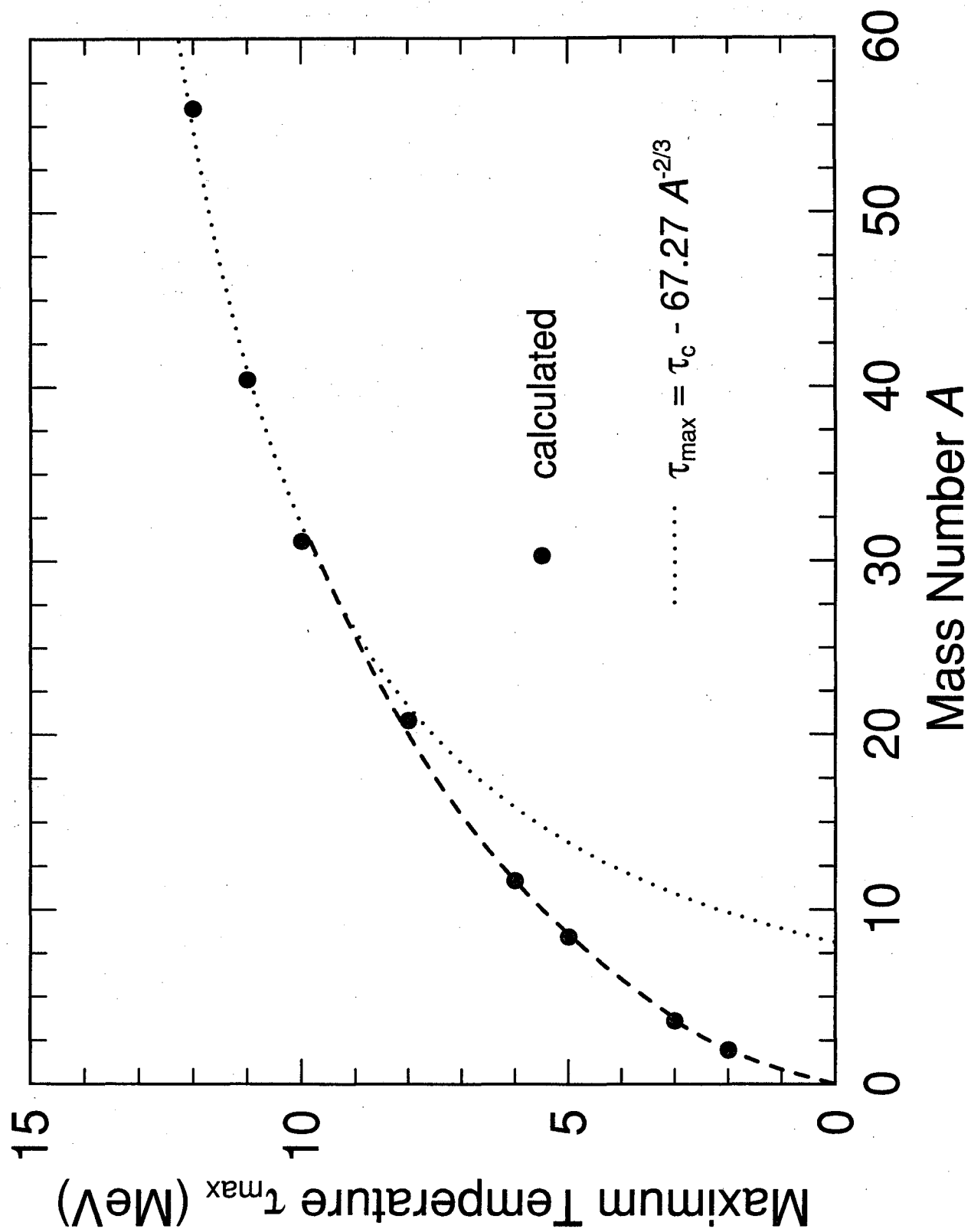
The temperature dependence of the volume and surface coefficients $a_1(\tau)$ and $a_2(\tau)$ in the liquid-drop expansion (26) for the free energy $F_A(\tau)$ of an excited nucleus embedded in a nucleon vapor held at a given temperature τ .

Figure 6: Multifragmentation barriers for ^{120}Sn

A system with 50 protons and 70 neutrons is represented as a symmetric configuration of N spherical fragments of equal size (see text for details). The figure shows the energies of the corresponding N -fragment systems, as functions of the *rms* size q of the total matter distribution, calculated at zero temperature. The vertical bars indicate the point at which the N spheres touch. For $N=12$, the open circles indicate the values corresponding to an alternative symmetric arrangement of the fragments. Furthermore, the dashed curve shows the result of a monopole distortion of ^{120}Sn .

Figure 7: Multifragmentation branching ratios

For the multifragment channels displayed in fig. 6, the corresponding outwards directed statistical currents $\nu_{A_1 \dots A_N}(E)$ given by eq. (39) are shown, as calculated at the top of the respective conditional potential barriers. The results have been divided by the binary current $\nu_{A_1 A_2}(E)$, so that the figure displays the branching ratios between the symmetric N -fragment breakups and a symmetric binary split.



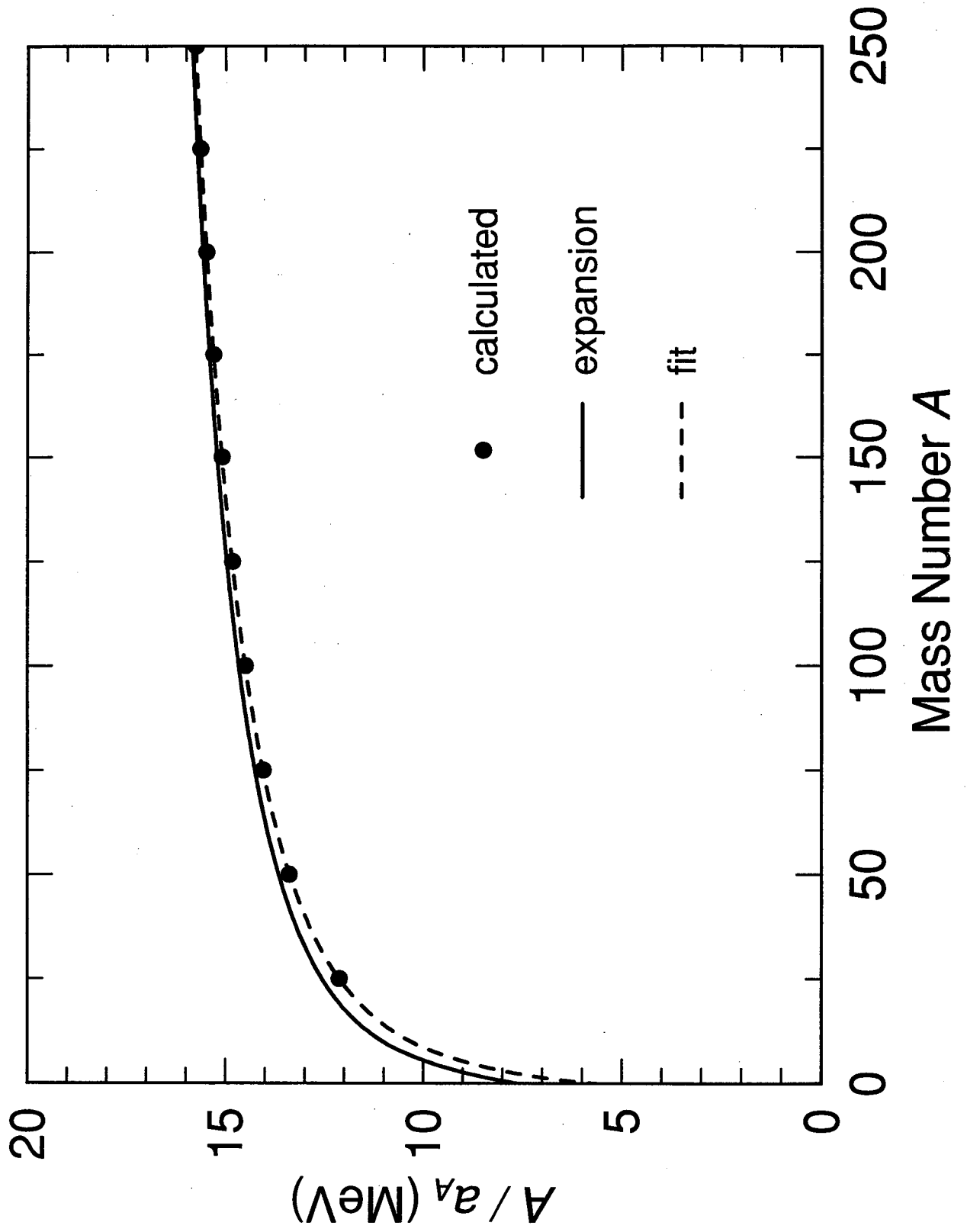


Figure 2

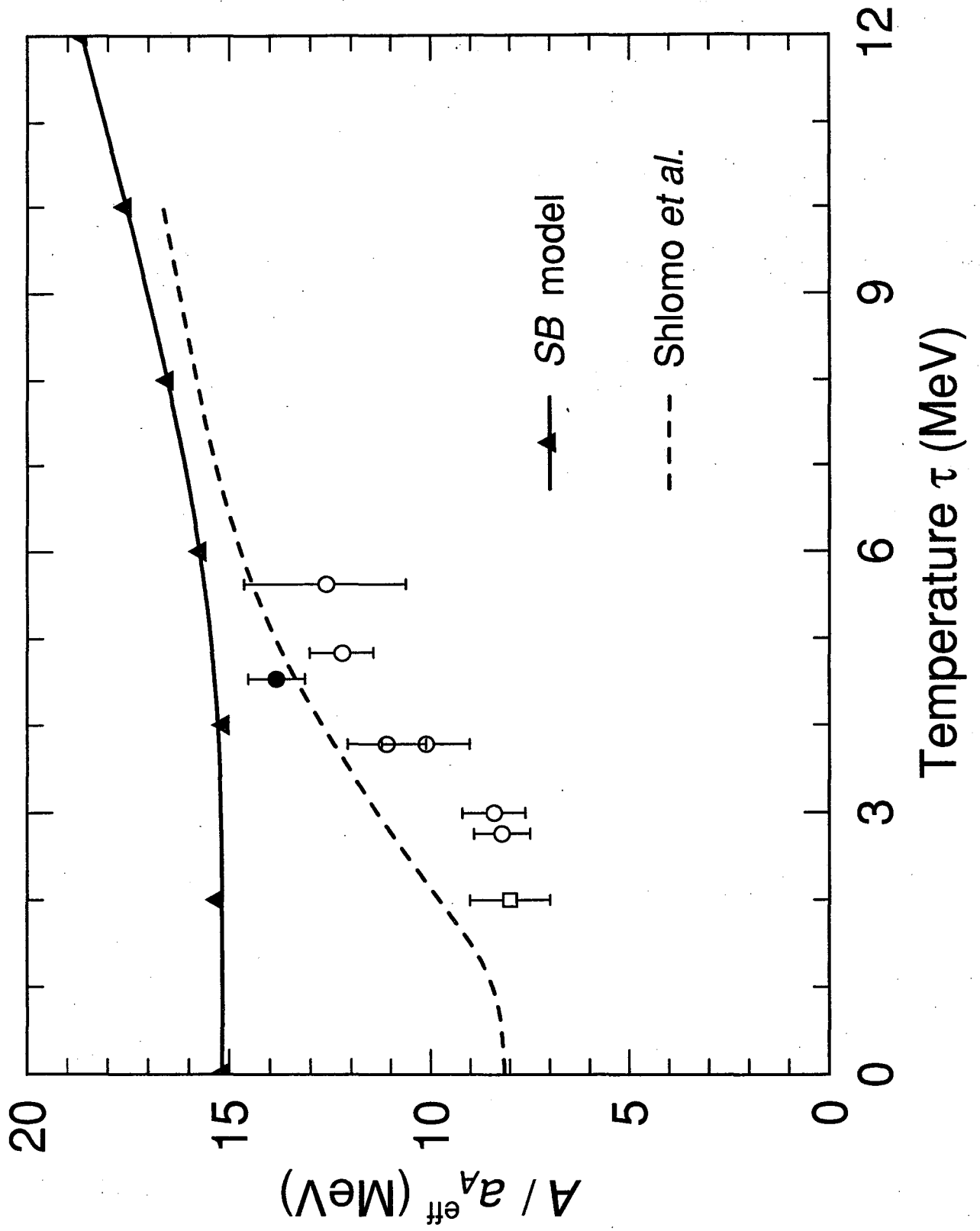
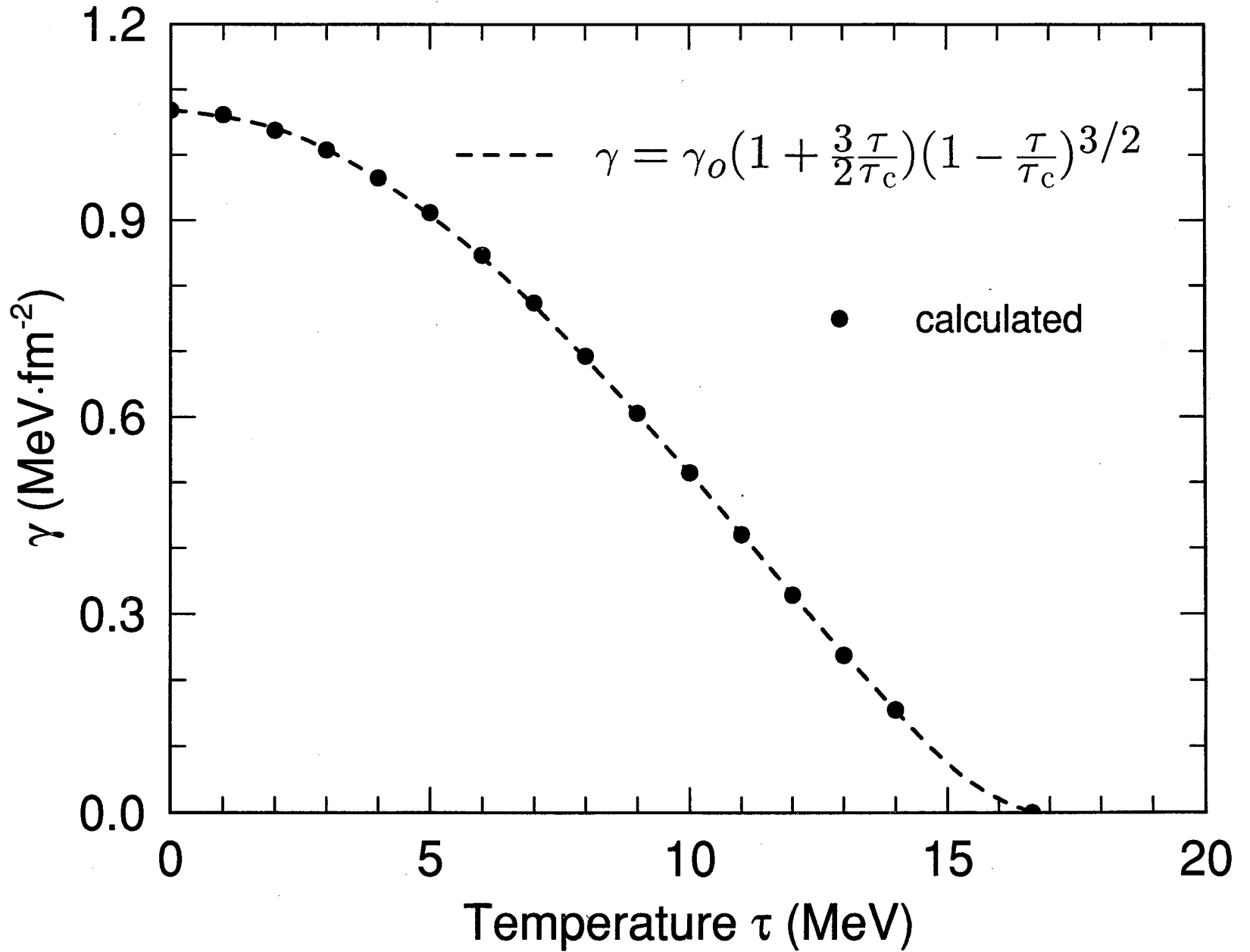


Figure 3

Surface Tension



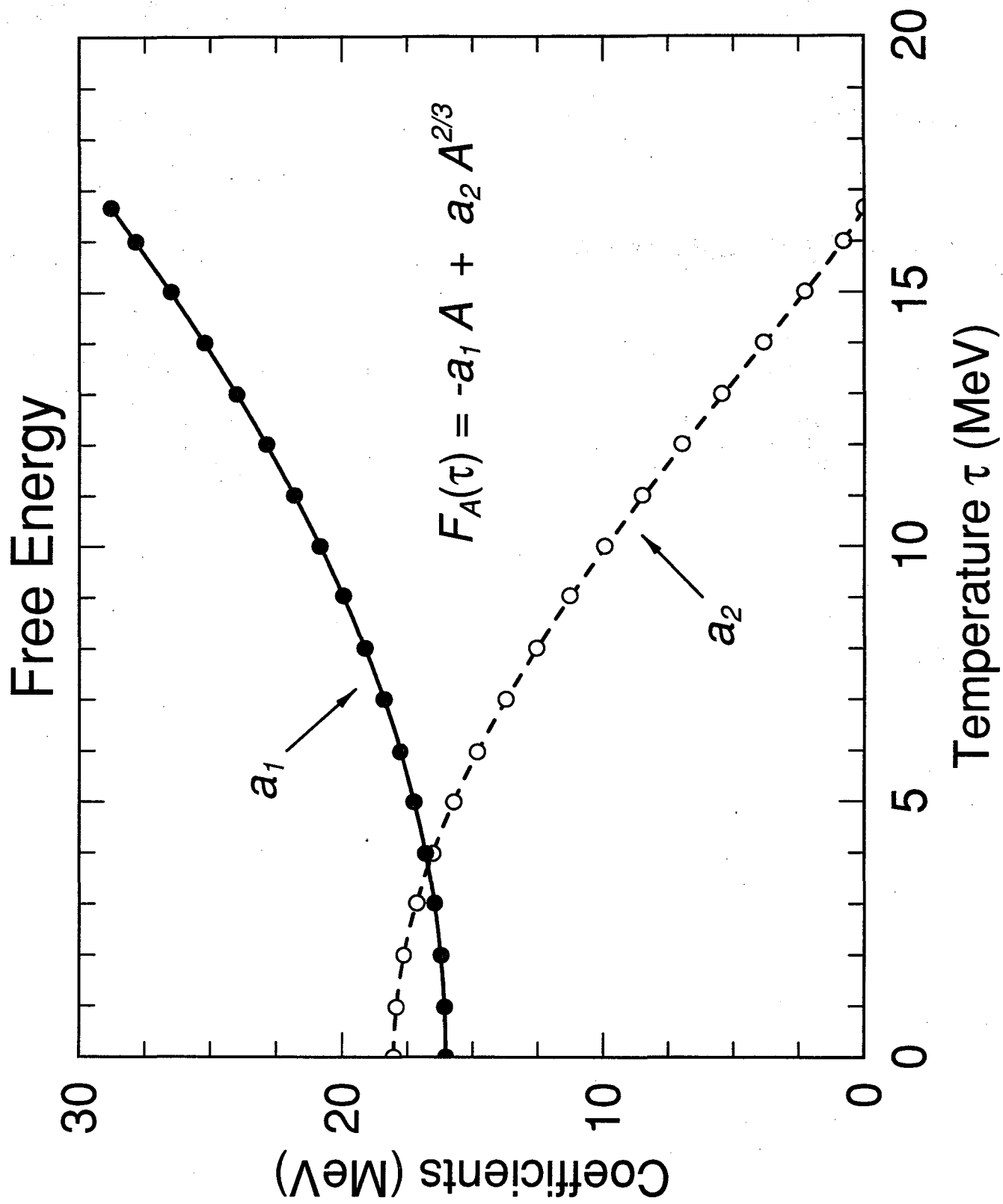
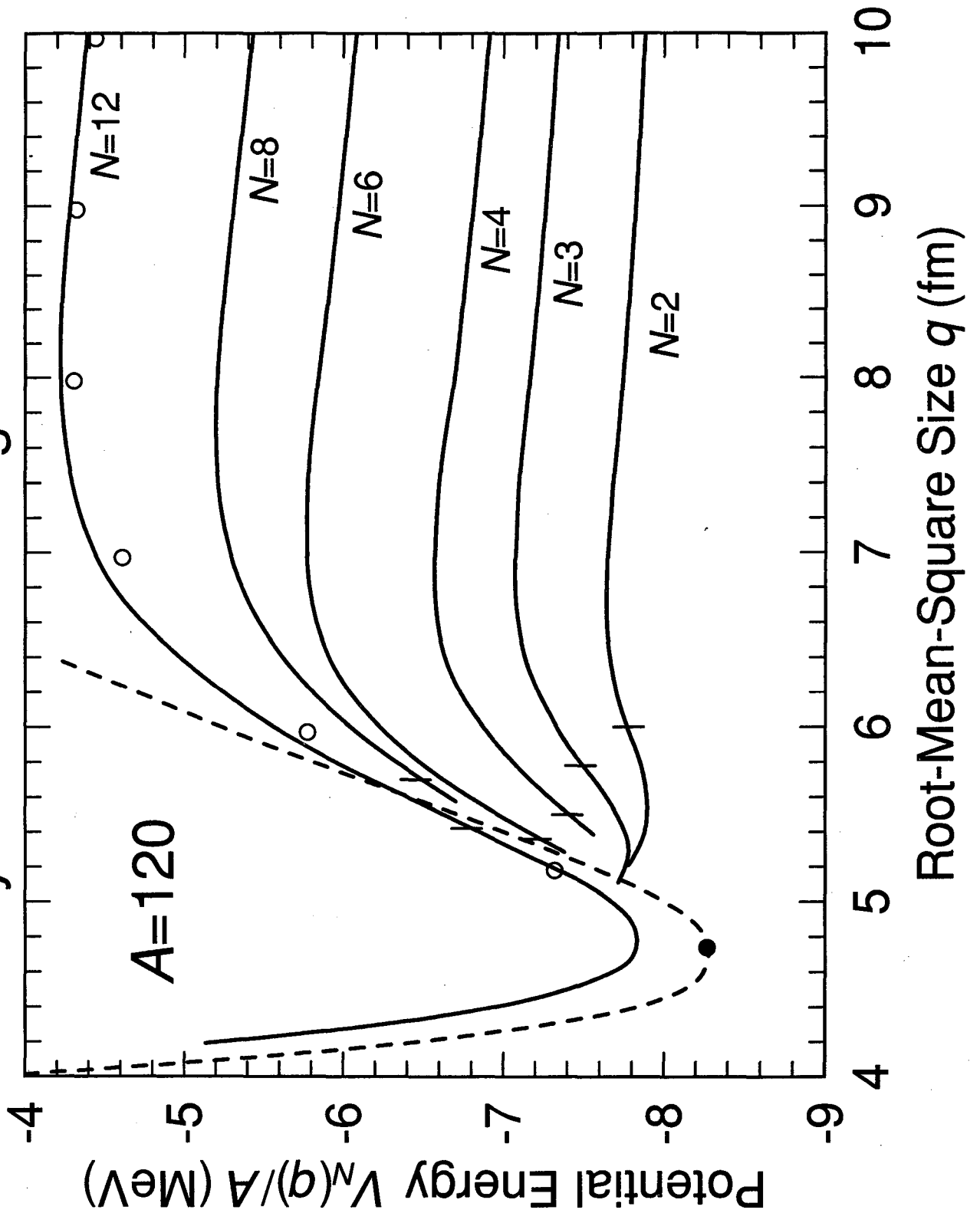
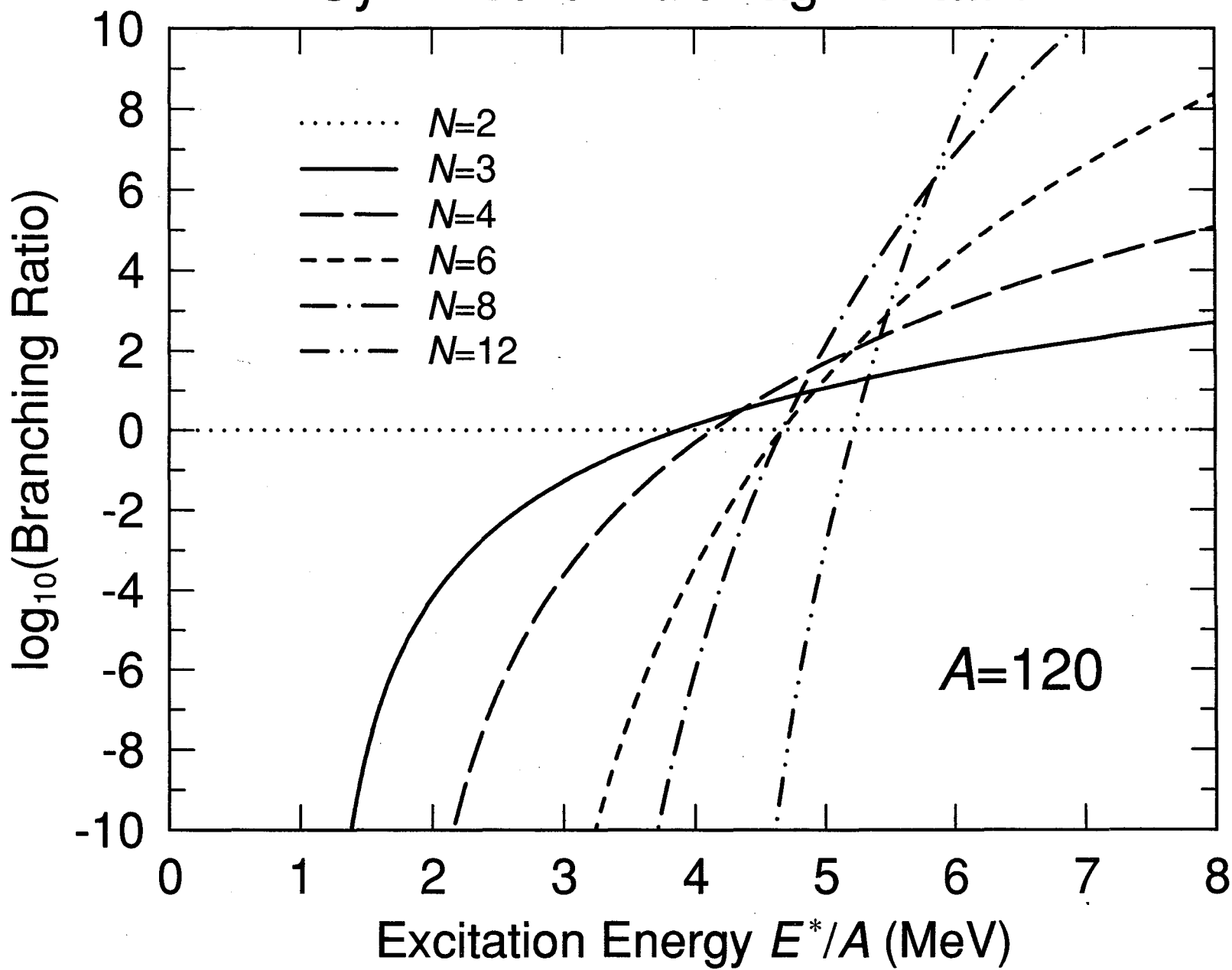


Figure 5

Symmetric Multifragmentation



Symmetric Multifragmentation



LAWRENCE BERKELEY LABORATORY
UNIVERSITY OF CALIFORNIA
INFORMATION RESOURCES DEPARTMENT
BERKELEY, CALIFORNIA 94720